

Satellite-derived Bathymetry for shallow coastal waters in Cyprus

Evagorou Evagoras^{1,2*}, Mettas Christodoulos^{1,2} and Hadjimitsis Diofantos^{1,2}

¹ Department of Civil Engineering and Geomatics, Faculty of Engineering and Technology, Cyprus University of Technology, 3036 Lemesos, Cyprus; ² Eratosthenes Centre of Excellence, 3036 Lemesos, Cyprus

ABSTRACT

During the last years, many studies related to Satellite-Derived Bathymetry (SDB) emphasize the potential use of optical satellite remote sensing sensors for bathymetric estimation. For this study, ten multispectral SPOT 6/7 satellite images with a medium resolution covering the coastal waters of the study areas were analyzed. These images were geometric, radiometric, and atmospheric corrected and acquired in three different sensing dates having coverage with at least 30% of lidar data. A number of 5284 random depth measurements with 0 to 50 meters depth were acquired for the ratio conversion algorithm with absolute depths and error assessment.

A series of steps were performed to obtain reliable results using satellite optical data such as, sun glint process, land/sea extraction, kernel filters. The study area was divided into three sub-regions, based on the sensing date of the satellite imageries. The light attenuation in the water column increases at a depth of about thirty meters as seen in other related studies. This study identified the depth of light attenuation to determine the maximum depth that can be estimated through optical sensors. The results show that better correlation was identified up to 15 meters depth. Results of the regression analysis show the following correlation coefficients R^2 : 0.90, 0.87, 0.80, and 0.89 with the Root Mean Square Error (RMSE) for the respective study areas to be 1.34, 1.53 1.70 and, 1.15.

Keywords: Satellite-Derived Bathymetry, Ratio transform algorithm, SPOT 6/7, Optical Remote Sensing, Marine Spatial Planning

1. INTRODUCTION

The determination of Bathymetry is valuable for maritime and land activities related to Marine Spatial Planning (MSP). This approach is expected to provide multiple benefits for MSP because with very low cost will be able to redefine the seabed and provide bathymetric information for areas that are not currently available. The estimation of the bathymetrical data is considered as a crucial component for an integrated MSP. Activities and land use at the bottom of the sea, sea column and sea surface should be classified to implement the maps of conflicts and synergies.

Bathymetry can be estimated using various techniques with different accuracy, errors, advantages, disadvantages, etc. Traditional methods for visualizing underwater topography mainly use echo sounds techniques which are divided into two categories; (a) Single Beam Echo Sound (SBES) providing high accuracy with less coverage and; (b) Multi-Beam Echo Sound (MBES) that provides the highest accuracy and coverage [1–3]. An additional, new modern technique that was adopted in recent years concerns active sensors – LIDAR systems. The systems may be installed on aerial platforms, remote-controlled vehicles (RV's), and autonomous underwater vehicles (AUV's). The operating cost of this technique, for the extraction of underwater topography, is very high, which has led researchers to look for alternative methods of estimating depth [4]. Space technology has offered cost-effective alternative means of mapping near coastal waters [5].

The assessment of depth through satellite data is named as Satellite-Derived-Bathymetry (SDB) and was appeared in the early of 1970s, when multiband satellite sensors such as the Landsat satellite began orbiting the Earth [6]. One of the active sensors, the Synthetic Aperture Radar (SAR), was used to estimate Bathymetry [7,8]. Nevertheless, studies using passive sensors such as the multispectral [9,10], and the hyperspectral sensors [11–13] became more prevalent in the scientific community, which performed many studies and techniques.

Based on the theory that the intensity of electromagnetic energy gradually weakens as depth increases due to the Inherent Optical Properties (IOPs) of the water column in the coastal area, the estimation of Bathymetry can be achieved using passive sensors. SDB is possible to be derived by using existing in-situ depth data, the theory of underwater reflectance,

underwater optics and algorithms [14]. Thus, using multi/hyper-spectral sensors that provide a wide range of wavelength zones with predefined models can achieve the Bathymetry estimation. The main bands used on those models are the Green and Blue ones, penetrating up to 25 meters below sea level into clear waters [15]. Several methods were used to achieve the assessment of SDB, categorized into empirical [16,17], semi-empirical [18], analytical [19], semi-analytical [20–22] and quasi-analytical [23–25]. Also, a numerous of studies used different sensors on SDB over the past 50 years, using evolving algorithms and approaches.

Furthermore, empirical methods require less constraints than analytical methods, as only in-situ depth points are needed. In contrast, analytical methods require spectral signatures of the water column and the different types of sea substrates [26]. Thus, the main advantage of the empirical methods is that they can adopt for each selected band without taking into account the physical-visual properties [27]. Many of these empirical methods used by researchers from all over the world, such as simple linear regression analysis [28], linear ratio [29], multiple linear regression polynomial of ratio transform [30], Least Squares Boosting Fitting Ensemble [31], Support Vector Regression [32] etc.

Bathymetry is a significant component to be defined for the whole island of Cyprus for the design and implementation of MSP. In the framework of this study, the assessment of the Bathymetry is presented using empirical methods and optical satellite data (SPOT 6/7) for the shallow coastal waters of the island of Cyprus. The challenge of this study was to examine the use of a calibration equation, derived using an empirical model of an area with known depth through (in-situ data), to find the bathymetry of areas with unknown depth data, using a set of satellite imagery with the same date of reception. The next part of the study describes the field data sets as well as the details of the used satellite images. Then a detailed methodology for the production of bathymetric maps is given. Next, the results of bathymetric maps and the accuracy of each dataset can be found, while a first approach is made to estimate Bathymetry in areas where there are no in-situ depth data by applying the calculated calibration equations.

2. STUDY AREA AND MATERIALS

2.1 Study Area

This study concerns the coastal area of Cyprus and extends up to five and a half kilometers from the coastline to the sea. Cyprus has a strong Mediterranean climate with warm, dry summers, rainy but variable winters and in autumn and spring the weather conditions change rapidly. The winds are usually light to moderate and rarely unstable in Cyprus [33].

The coasts of Cyprus range from steep rough rocks and rocky shores with sea caves to quiet sandy beaches. Soft sand and gravel substrate in shallow water and fine sand, muddy sand and mud in deeper waters characterize the main bays of the south and east coasts. The type of substrates of the seabed of Cyprus can be classified into two broad categories, those associated with hard substrates and those of soft substrates. However, there is a complete gradient between the two, as many areas of the seabed include mixtures of hard and soft substrates [34].

A buffer zone was chosen to cover the entire area where in-situ depth data range up to 50 meters. The study area on the island of Cyprus is divided into two areas. The area where in-situ depth data are available (Figure 2.1- green color) and area where there are no available in-situ depth data Figure 2.1- red area).



Figure 2.1: Area of study

2.2 In-situ depth data

The in-situ depth data used in SDB to assess the accuracy of the bathymetric maps was provided by the Department of Lands and Surveys (DLS)[35]. DLS is the official provider of geographical data of the country. This data was obtained from the DLS in three phases. The first phase used a multibeam echo sounder on a conventional vessel which collected bathymetric data for two hundred thirty-eight square kilometers by applying the Order 1b method in 2012. The second phase was carried out in 2014 using the LIDAR method installed on an aircraft using the Order 1b method by collecting two hundred seventy square kilometers of bathymetric data. The final phase was carried out in 2018 using the Order 1a method and covering the remaining area [36]. Figure 2.2 shows the areas and the phase that provided in-situ depth data the DLS.

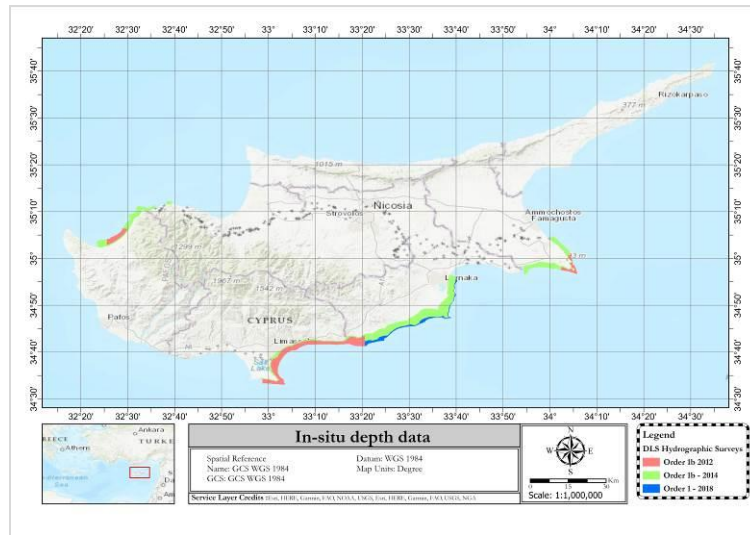


Figure 2.2: In-situ depth data provided by DLS

DLS provided 5282 random depth measurement points ranging from 0 to 50 meters of our study area. These depth data are used to (a) estimate the maximum ratio value for best results, (b) the ratio conversion algorithm, (c) and error assessment. It is worth noted that 30% of the points were kept to estimate the errors. The basic characteristics of the in-situ depth data provided by DLS can be seen in Table 1.

Table 1: Horizontal and vertical accuracies of the In-situ depth data provided by DLS

Hydrographic Surveys / Depth	Number of in-situ depths points	Methods of hydrographic surveys	Horizontal Accuracy (m)	Vertical Accuracy (m)
YA 2012 / 0-50	1654	Order 1b	0.6 - 0.8	0.5
YA 2014 / 0-20 m	2135	Order 1b	0.4	0.2
YA 2014 / 20-50 m	1017	Order 1b	0.4	0.6
YA 2018	476	Order 1a	0.1 - 0.8	0.1 - 0.8

2.3 Satellite data

The present work utilizes a set of imageries data captured by the SPOT 6/7 satellites. SPOT 6/7 satellites are the upgrade of the SPOT 5 satellite (shut down in 2015), using new improvements from the PLEIADES 1 & 2 program. The SPOT 6/7 spacecraft operates alongside DLR's TerraSAR-X (TSX) and TanDEM-X (TDX) radar satellites. The sensors of SPOT 6/7 have five bands, the panchromatic (0.455 μm to 0.755 μm) with 1.5 meters spatial analysis and four

multispectral bands with 6 meters spatial analysis, including: blue (0.455 μm - 0.525 μm); green (530-590nm); red (625-695nm) and near-infrared (0.760-0.890 μm) [37].

For the purpose of this study, multispectral imageries of the SPOT 6/7 are required, covering all areas that lack of in-situ depth data. Additional multispectral imagery was needed for each acquired multispectral imagery where in-situ depth data was available with the same sensing date. Also, these imageries had a minimum coverage of 30% (compared to the corresponding area) for calibration purposes. Figure 2.3 shows the plotting of the satellite images with the table below with the serial number (ID) corresponding to the satellite image. Table 2 presents the details of satellite imageries that were used to derive SDB in Cyprus.

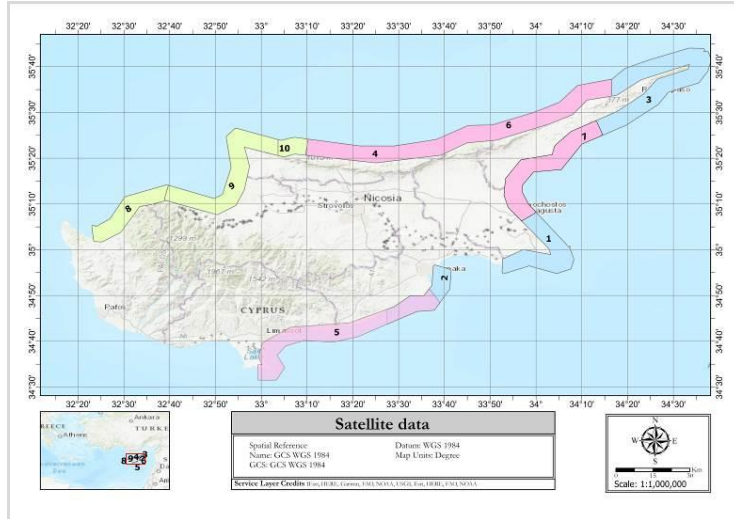


Figure 2.3: IDs of Satellite images

Table 2: Details of SPOT Satellite imageries

ID	Name	Date Acquisition	Orientation angle	Incidence angle	Sun Azimuth	Sun Elevation
1	DIM_SPOT7_MS_201611180801272_PRJ_4232653101	18/11/2016 (08:01)	+114.08°	+17.51°	+154.79°	+32.04°
2	DIM_SPOT7_MS_201611180801272_PRJ_4232683101	18/11/2016 (08:01)	+119.83°	+15.02°	+155.26°	+32.00°
3	DIM_SPOT7_MS_201611180801127_PRJ_4232684101	18/11/2016 (08:01)	+94.28°	+13.05°	+155.67°	+31.55°
4	DIM_SPOT7_MS_201712250807529_PRJ_4232646101	25/12/2017 (08:08)	+14.31°	+19.43°	+155.48°	+26.88°
5	DIM_SPOT7_MS_201712250808581_PRJ_4232647101	25/12/2017 (08:09)	+167.78°	+14.86°	+154.76°	+27.23°
6	DIM_SPOT7_MS_201712250807529_PRJ_4232645101	25/12/2017 (08:08)	+21.96°	+19.96°	+155.21°	+26.64°
7	DIM_SPOT7_MS_201712250808581_PRJ_4232644101	25/12/2017 (08:09)	+169.34°	+15.42°	+155.01°	+26.77°
8	DIM_SPOT6_MS_201804140813259_PRJ_4232691101	14/04/2018 (08:13)	+178.04°	+14.99°	+134.08°	+55.32°

9	DIM_SPOT6_MS_201804140813259_ PRJ_4232689101	14/04/2018 (08:13)	+184.64°	+15.43°	+134.65°	+55.32°
10	DIM_SPOT6_MS_201804140813089_ PRJ_4232690101	14/04/2018 (08:13)	+199.99°	+5.51°	+135.01°	+55.49°

3. METHODOLOGY

The methodology chapter describes the steps for estimating SDB using optical images and in-situ depth data for the coastal area of Cyprus. In the first step, the deep-sea data was collected and separated from the Land Registry. This data was divided into two packets, in-situ depth data for calibration purposes (70%) and in-situ depth data for validation purposes (30%).

The second step concerned the selection of satellite images covering a) areas with in-situ depth data and b) areas with no in-situ depth data. These optical imageries should have a common sensing date and a minimum coverage of 30% (compared to the corresponding area) for calibration purposes. Ten multispectral images of the SPOT 6/7 were used, geometrically, radiometrically, and atmospherically corrected by the provider.

The Normalized Difference Water Index (NDWI) for land/sea separation was used in the third step as seen in equation (1). This step must be applied to avoid the effect of land pixel with the water pixel during the implementation of the bathymetric algorithm [38].

$$NDWI = \frac{GREEN - NIR}{GREEN + NIR} \quad (1)$$

where, GREEN is a band that encompasses reflected Green light and NIR represents reflected Near-Infrared Radiation.

The fourth step followed was the application of a 3x3 median filter for each satellite image to achieve high-frequency noise reduction. The median filter is often used to remove noise from other false characteristics of the area of a pixel, while maintaining the overall quality. Otherwise, low-pass filters will only blur noise instead of removing it [39]. Thus, a median filter is applied to achieve noise reduction due to turbidity, waves, etc.

To estimate Bathymetry in areas with no in-situ depth data, the values of electromagnetic energy of the ratio value of two bands in each satellite image (where the absorption of electromagnetic energy begins) should be calculated, to define the boundaries of SDB maps. As Stumpf stated [29], the reflectance of each band of satellite images has different water absorptions, as a result, the ratio will change with depth. Log-transform represents the exponential reduction of light penetration with depth according to Beer Law [26]. Different types of bottoms (substrates) at the same depth have about the same proportion values. Therefore, to remove substrate variability, one can use the ratio of two different wavelengths [17]. Thus, considering that the substrate does not affect the ratio of two different wavelengths for each depth, the first stage was to identify the values (W_i) where the absorption of electromagnetic energy decreases and alters the depth effects. The equation (2) for determining these values can be seen below:

$$W_i = \frac{\log(bx)}{\log(by)} \quad (2)$$

where, W_i is the ratio of the corrected values of the Blue band (bx) with the Green band (by).

The sixth step was the application of linear ratio algorithm, using only the points with estimated maximum W_i . The linear ratio algorithm provides the calibration equations to be applied to the areas with no in-situ depth data. The equation below shows the linear ratio algorithm used for all satellite imageries with in-situ depth data:

$$Z_{SDB} = m_1 \frac{\log(bx)}{\log(by)} - m_0 \quad (3)$$

where Z_{SDB} is the SDB depth, m_0 and m_1 is a coefficient to tune the model to the actual depth, and b_x and b_y are the corrected values of radiances for optical bands (b_x = blue band and b_y =green band).

The seventh step was the estimation of the correlation coefficient (R^2) and the assessment of the statistical parameter of the Root Mean Square Error (RMSE) for each study area. The equation below shows the RMSE equation:

$$RMSE = \sqrt{\frac{1}{n} \sum_{j=1}^n (Z_{SDB} - Z_{IDD})^2} \quad (4)$$

The eighth step concerned the estimation of Bathymetry for the areas with no in-situ depth data, using the calibration equations to the corresponding satellite images with the same sensing date. The results provide the bathymetric maps for all satellite images and are presented in the following chapter. Figure 4 shows the aforementioned processing steps for deriving Bathymetry in the study area.

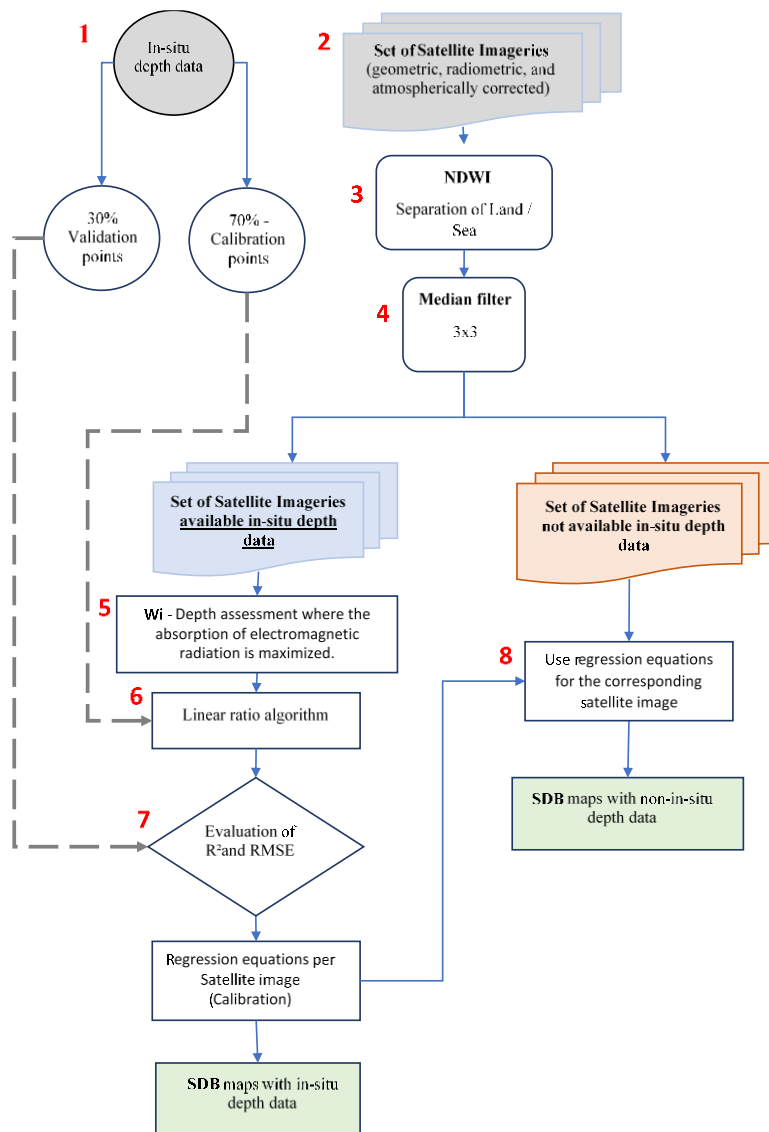


Figure 4: Workflow processing steps of SDB using SPOT 6/7 satellites images

4. RESULTS

Following the above methodology, the maximum value of W_i was estimated when the absorption of electromagnetic radiation was maximized. Four bathymetric maps were created using in-situ depth data, and calibration equations were noted. Following regression analyses, the coefficient of determination (R^2) and the RMSE were calculated using the validation points reserved for validation. Also, a first approach of SDB with no in-situ depth data was made, creating six bathymetric maps.

4.1 Estimation of the maximum value of W_i


This section presents the results concerning the estimation of the maximum value of W_i , the depth where the absorption of electromagnetic radiation was maximized, and the correlation observed with the field data. By subtracting the W_i values observed the absorption of electromagnetic energy, an improvement was stated.

A significant step of the processing was the creation of the W_i line. The W_i line was created by interpolation with the help of ArcGIS pro software using the W_i values of each satellite image. The W_i line aims to identify the number of points below fifteen meters that do not fall within this line; the W_i line set the limit of SDB maps for areas where there is no in-situ depth data.

Table 3 shows four scatterplots of W_i values against in-situ depth points. These scatterplots reveal that the maximum estimated Bathymetric depth is fifteen meters. On the third column of the table, you can see the maps with the final in-situ depths data used for calibration with green color ($Z \geq -15$ meters), the in-situ depth data that is not used with yellow color ($Z < -15$), and the W_i line created by interpolation (Redline). The fourth column show the results of the W_i processing values.

Table 3: Estimation of the maximum value of W_i and the maximum depth for the calibration points

ID	Scatterplots of W_i / in-situ depth points	W_i / remaining in-situ depths points for calibration	Results of W_i processing
1			$W_i = 1.108$ No of in-situ depth points used for calibration = 188 Number of the removed in-situ depth points = 407
2			$W_i = 1.108$ No of in-situ depth points used for calibration = 622 Number of the removed in-situ depth points = 601
5			$W_i = 1.094$ No of in-situ depth points used for calibration = 1039 Number of the removed in-situ depth points = 1528


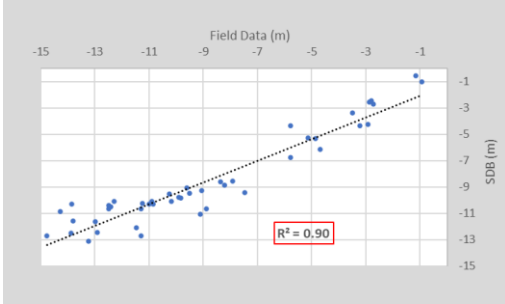
8			$W_i = 1.062$
	No of in-situ depth points used for calibration = 326		
	Number of the removed in-situ depth points = 328		

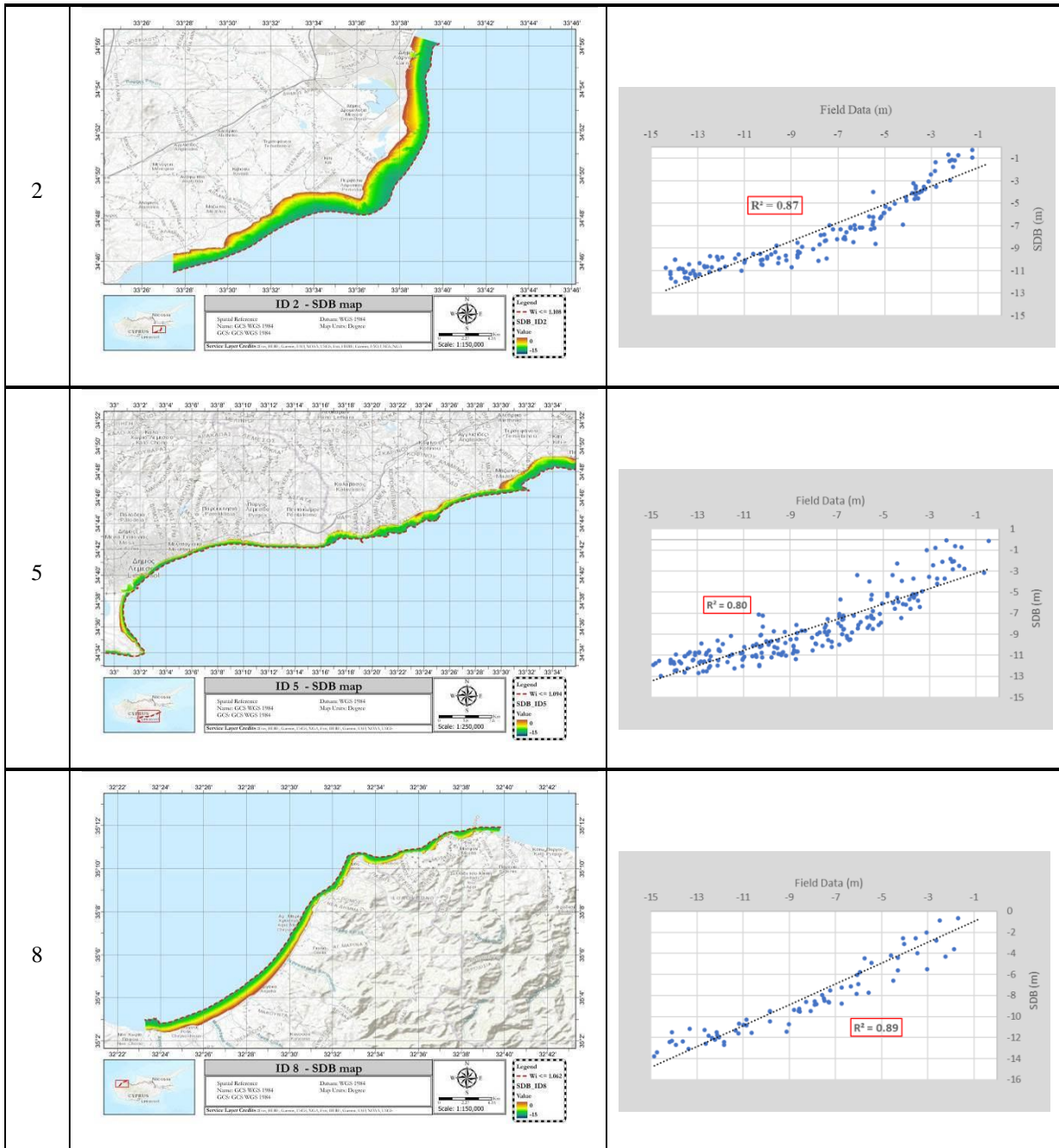
As shown in Table 3 the satellite imageries with the same sensing date on different areas have the same value of W_i (ID 1 and ID 2). Also, the number of calibration and validation points was reduced to half. Furthermore, very good consistency of the W_i lines with varying sensing dates was noted. This state helped in the determination of the limits of the bathymetric maps extracted through calibration equations. However, some pixels observed on the limit line have higher values than the set maximum value, and this is probably noted due to the interpolation and smooth method used to retrieve the W_i line.

4.2 Bathymetric maps using in-situ depth points

This section presents the bathymetric maps using satellite images and field data. The bathymetric maps were created using the empirical methods. More specifically, Stumpf's linear ratio algorithm and the calibration points used in the previous section were used. In the assessment of the depth, the calibration equations for each satellite image were noted. Then, using the validation points for each satellite image, regression analyses, coefficient of determination (R^2), and the RMSE were calculated for each satellite image. The second column of Table 4 shows the bathymetric maps, while the third column shows the points used to equalize the calibration.

Table 4: Bathymetric maps and regression analysis with the SDB and validation of in-situ depth data

ID	Bathymetric Maps	Scatterplots
1		



The final step concerns the estimation of the error using the validation points for each area. The overall results regarding the RMSE errors can be found in Table 5. As resulted from the table below, the best results can be found on the satellite imagery with Id 8 where the Bathymetry resulted with RMSE to be 1.15 m. On the other hand, the less precise results having a RMSE of 1.70 m seem to be for the satellite imagery with Id 5.

Table 5: R², RMSE and calibration equations for each bathymetric map

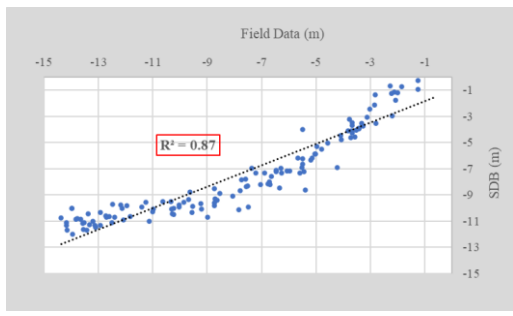
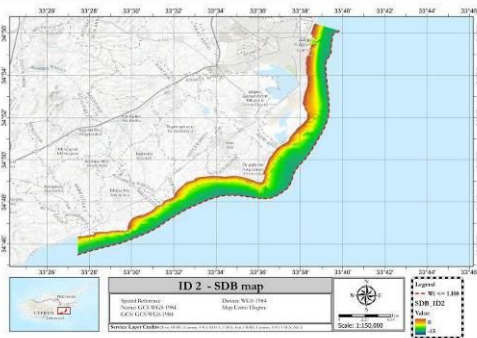
Id	Sensing Date	No. of Calibration points	Calibration Equation	R²	No. of validation points	RMSE (m)
1	18/11/2016	188	$Y = -88.83x + 86.87$	0.90	54	1.34
2	18/11/2016	622	$y = -146.28x + 151.01$	0.87	134	1.53
5	25/12/2017	1039	$y = -164.53x + 168.82$	0.80	200	1.70
8	18/04/2018	326	$y = -206.28x + 208.06$	0.89	77	1.15

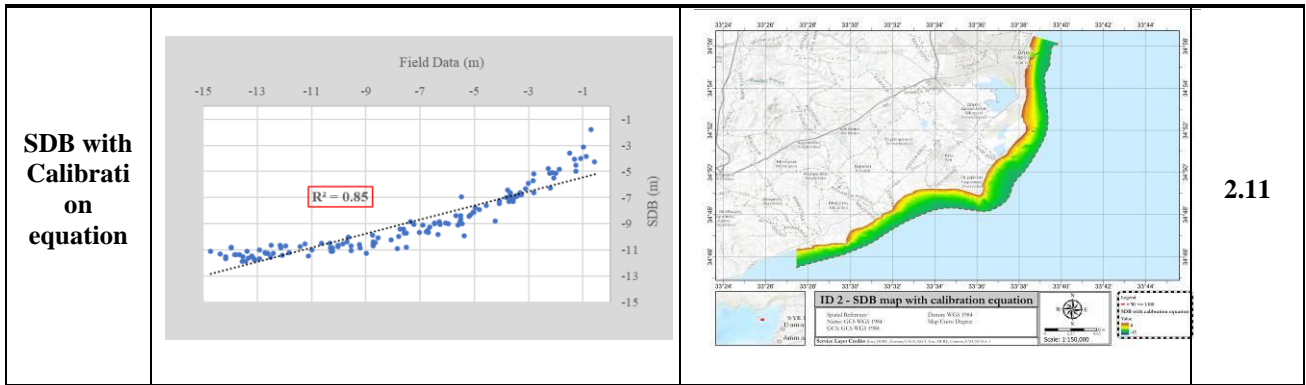
4.3 Estimate Bathymetric maps with no in-situ depth points

This section determines the estimation of Bathymetry for the areas with no in-situ depth data, using the SDB calibration equations on the corresponding satellite images with the same sensing date. To define the effect of the calibration equation on the SDB, boundaries were set using the Wi line. The same maximum Wi values were used for imagery with the same sensing date for each satellite imagery.

Satellite images with IDs 1 & 2 have the same sensing date and availability of in-situ depth data. In this section, the aspect considered that the image with ID 2, in-situ depth data are not available and was calibrated with the estimated equation of the satellite image with ID 1. The in-situ data for the image with ID 2 was used only for validation. The SDB results were compared using the validation points of the area as well as the SDB results using the Ratio transform algorithm compared with the SDB results using the calibration equation. It is worth noted that Wi values set in both satellite images at 1,108 as shown in Table 3. Table 6 indicates the results with the regression analysis diagram shown in column 2, the SDB maps in column 3 and the RMSE in column 4. As it can be seen from the bathymetric maps in column 3, there is a deviation in shallow waters. Additionally, the RMSE using the calibration equation is 38% greater than SDB using the ratio algorithm, with the difference between the two being 0.58 meters.

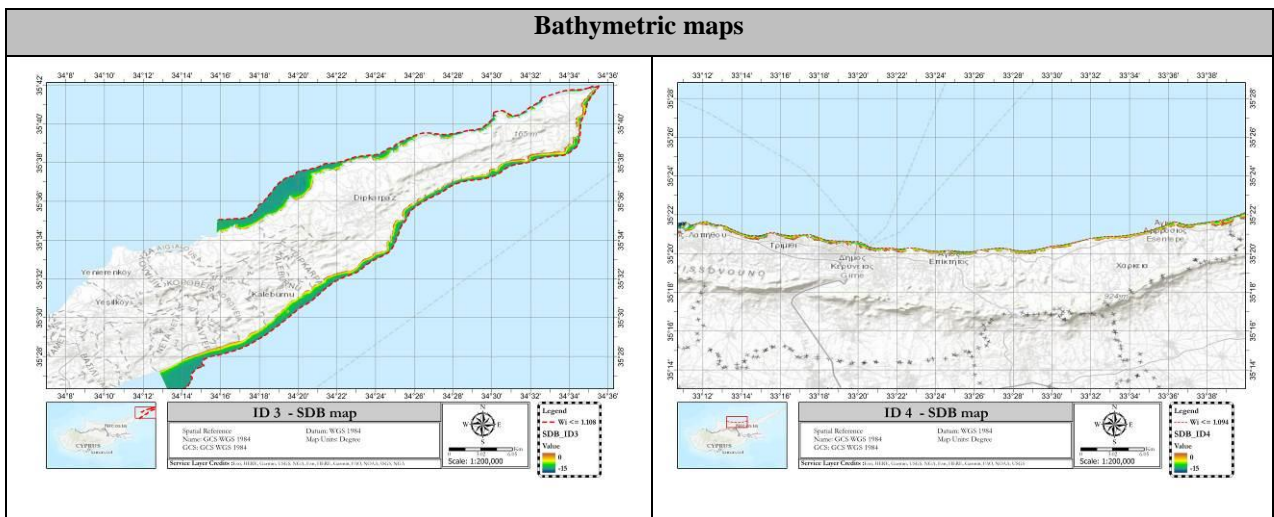
Table 6: Compared results using Ratio transform algorithm and calibration equations

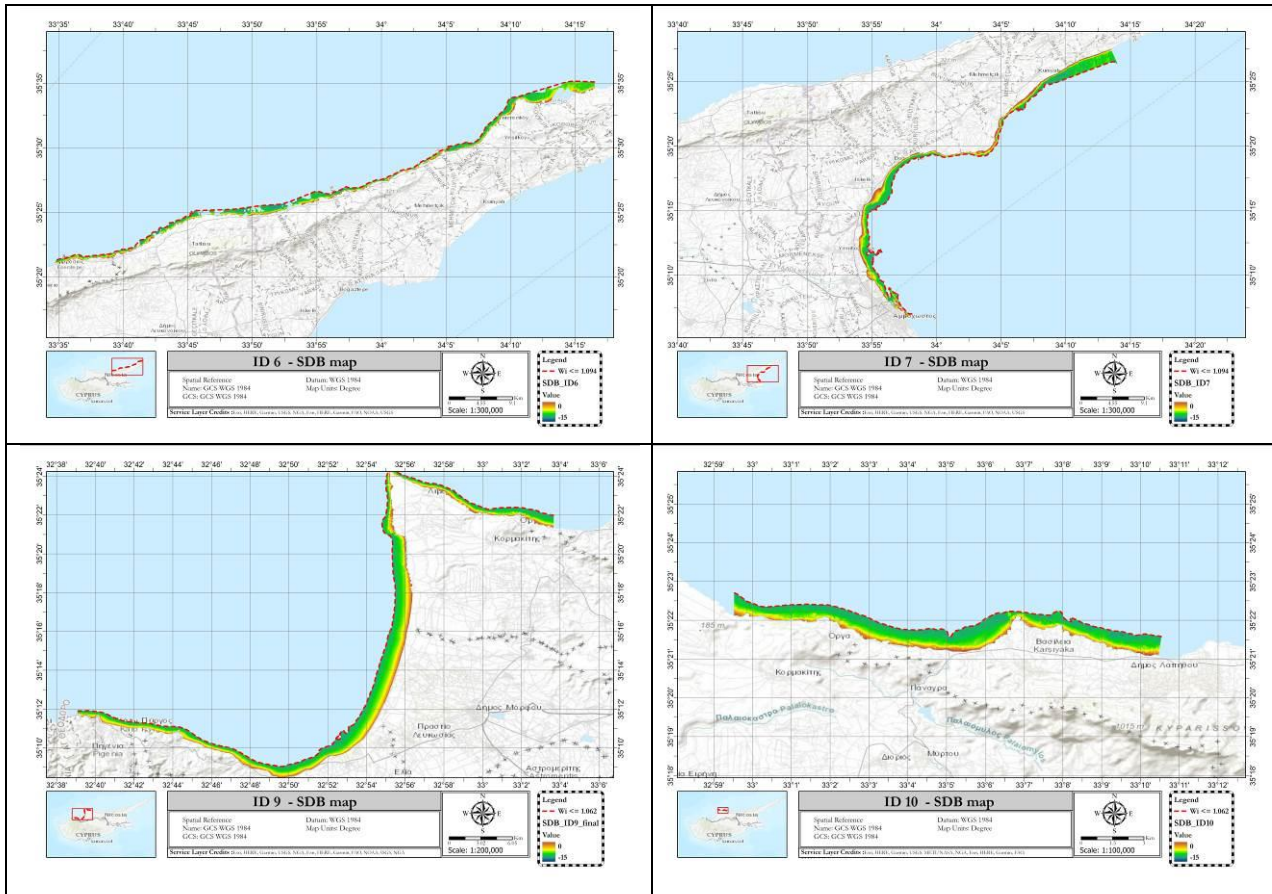
Method	Scatterplots of Wi / in-situ depth points	SDB maps	RMSE (m)
SDB with ratio transform algorithm			1.53



Upon completion of the above comparison, the estimation of SDB was followed using the calibration equations in areas where bathymetric data is not available. As shown in Figure 2.3, ID3 imagery has the same sensing date with the imageries with ID 1&2, imageries with ID 4,6&7 correspond with the ID 5 imagery, and the final set of imageries with ID 9&10 correspond with the imagery with ID 8. This set of satellite imageries with no in-situ depth data used the SDB calibration equation and the W_i values of the corresponding satellite imagery of the above Table 5. Since the field data were not available in these areas, the accuracy of the results cannot be estimated. The results of bathymetric maps using the calibration equation can be found in Table 7.

Table 7: Estimated bathymetric maps using the calibration equation from the corresponding satellite imageries





The fact that field data are not available for the above areas leads in the conclusion that the accuracy of the results cannot be estimated. It is worth noting that these bathymetric maps are preliminary as further analysis with different algorithms will be carried out and SDB will be performed using other sensors.

5. DISCUSSION CONCLUSION

Earth Observation sensors are an important informative tool for local stakeholders and other interested parties, providing reliable and up-to-date information for land and sea areas. Remote sensing can play an important role in the frame of MSP, as this technology provides frequent, inexpensive, and accurate information on large areas. Bathymetry has an important role in MSP. This study aimed to estimate Bathymetry using optical images for areas where in-situ depth data are not available.

On the current study, an attempt was made to estimate Bathymetry without using field data. Ten satellite images of SPOT 6/7 were used, four to estimate calibration equation and six to apply and estimate Bathymetry for areas where in-situ depth data was unavailable. Also, an estimation of the maximum depth where the SDB can be implemented (water depth not exceeding 15 m) was determined. Moreover, for each satellite image with a different sensing date, an estimation was made of the maximum value of W_i to identify the point where the absorption of electromagnetic energy begins, decreases and alters the depth effects. Through the W_i lines, consistency observed at fifteen meters depth despite the difference of W_i values.

For the first set of imagery analysis, the overall results indicate an error ranging from 1.15 m up to 1.70 m. The results of this study are considered acceptable based on other similar studies carried out by empirical methods. The correlation between situ data and predicted depths is not ideal and may be due to the sensing date of satellite imagery.

The estimation of Bathymetry was followed by applying the calibration equations where field data were not available, considering the use of satellite images having the same date of sensing date. These images were radiometrically,

atmospherically, and geometrically corrected images. The linear ratio algorithm was used, with a very important assumption of this algorithm which considers that there is no substrate effect.

However, this article contains some limitations. The weather conditions and the sea currents on the different areas of the island are different. Clean water and water quality also have an important role in the assessment of depth by empirical methods and the use of multispectral satellite images as it significantly increases the accuracy of the assessment of depth. Due to extensive areas and distances between the areas of studies, water quality and weather conditions may be different. Also, the fact that field data are not available in some areas can not estimate the accuracy of the results. It is worth noting that these bathymetric maps are preliminary as further analysis with different algorithms will be carried out and SDB will be performed using other sensors as well.

ACKNOWLEDGEMENTS

This research was supported by project entitled: “Cross-Border Cooperation for Implementation of Maritime Spatial Planning” referred as “THAL-CHOR 2” (“ΘΑΛ-ΧΩΡ 2” in Greek) and is co-funded by the European Regional Development Fund (ERDF), under the Cross-Border Cooperation Programme “INTERREG V-A Greece-Cyprus 2014–2020”. This research is also part of the PhD Thesis of Evagoras Evagorou, hosted at the Remote Sensing and Geo-Environment Lab, of the Department of Civil Engineering and Geomatics of the Cyprus University of Technology, supported also by the ‘EXCELSIOR’ H2020 Teaming project. The authors acknowledge the ‘EXCELSIOR’: ERATOSTHENES: EXcellence Research Centre for Earth Surveillance and Space-Based Monitoring of the Environment H2020 Widespread Teaming project (www.excelsior2020.eu). The ‘EXCELSIOR’ project has received funding from the European Union’s Horizon 2020 research and innovation programme under Grant Agreement No 857510 and from the Government of the Republic of Cyprus through the Directorate General for the European Programmes, Coordination and Development. Also, acknowledgements are given to Department of the Land Survey of Cyprus, for providing soundings of Bathymetry.

REFERENCES

- [1] Wu, Z., Yang, F. and Tang, Y., “Multi-beam Bathymetric Technology,” *High-resolution Seafloor Surv. Appl.*, 21–76 (2021).
- [2] Marks, K. M. and Smith, W. H. F., “An uncertainty model for deep ocean single beam and multibeam echo sounder data,” *Mar. Geophys. Res.* 2009 294 **29**(4), 239–250 (2009).
- [3] Renjie, W. and Chengpeng, L., “Comparison and analysis of thinning methods for multi-beam sounding data” (2020).
- [4] Wright, W., Kranenburg, C., Battista, T. A. and Parrish, C., “Depth Calibration and Validation of the Experimental Advanced Airborne,” *Source J. Coast. Res.* **76**(sp1), 4–17 (2016).
- [5] Dierssen, H. M. and Theberge, A. E., “Bathymetry: Assessment,” *Encycl. Nat. Resour. Water*, 629–636 (2016).
- [6] Clark, R. K., Fay, T. H. and Walker, C. L., “Bathymetry Using Thematic Mapper Imagery,” *Ocean Opt.* IX **0925**, 229–231 (1988).
- [7] Pereira, P., Baptista, P., Cunha, T., Silva, P. A., Romão, S. and Lafon, V., “Estimation of the nearshore bathymetry from high temporal resolution Sentinel-1A C-band SAR data - A case study,” *Remote Sens. Environ.* **223**, 166–178 (2019).
- [8] Renga, A., Rufino, G., D’Errico, M., Moccia, A., Boccia, V., Graziano, M. D., Aragno, C. and Zoffoli, S., “SAR bathymetry in the Tyrrhenian sea by COSMO-SkyMed data: A novel approach,” *IEEE J. Sel. Top. Appl. Earth Obs. Remote Sens.* **7**(7), 2834–2847 (2014).
- [9] Pike, S., Traganos, D., Poursanidis, D., Williams, J., Medcalf, K., Reinartz, P. and Chrysoulakis, N., “Leveraging Commercial High-Resolution Multispectral Satellite and Multibeam Sonar Data to Estimate Bathymetry: The Case Study of the Caribbean Sea,” *Remote Sens.* 2019, Vol. 11, Page 1830 **11**(15), 1830 (2019).
- [10] Muzirafuti, A., Barreca, G., Crupi, A., Faina, G., Paltrinieri, D., Lanza, S. and Randazzo, G., “The Contribution of Multispectral Satellite Image to Shallow Water Bathymetry Mapping on the Coast of Misano Adriatico, Italy,” *J. Mar. Sci. Eng.* 2020, Vol. 8, Page 126 **8**(2), 126 (2020).
- [11] Cerra, D., Gege, P., Evagorou, E., Agapiou, A. and Reyes, R. de los., “Monitoring Marine Areas from the

- International Space Station: The Case of the Submerged Harbor of Amathus,” *Lect. Notes Comput. Sci. (including Subser. Lect. Notes Artif. Intell. Lect. Notes Bioinformatics)* **12642 LNCS**, 127–137 (2020).
- [12] Alevizos, E., “A Combined Machine Learning and Residual Analysis Approach for Improved Retrieval of Shallow Bathymetry from Hyperspectral Imagery and Sparse Ground Truth Data,” *Remote Sens.* 2020, Vol. 12, Page 3489 **12**(21), 3489 (2020).
- [13] Minghelli, A., Vadakke-Chanat, S., Chami, M., Guillaume, M., Migne, E., Grillas, P. and Boutron, O., “Estimation of Bathymetry and Benthic Habitat Composition from Hyperspectral Remote Sensing Data (BIODIVERSITY) Using a Semi-Analytical Approach,” *Remote Sens.* 2021, Vol. 13, Page 1999 **13**(10), 1999 (2021).
- [14] Polcyn, F. C. and Rollin, R. A., “Remote Sensing Techniques for the Location and Measurement of Shallow-Water Features,” *Proceedings of the Sixth Int. Symp. Remote Sens. Environ.*, 1–71 (1969).
- [15] Sutanto., “*Penginderaan Jauh Jilid 2*,” Gadjah Mada Press. Yogyakarta (1992).
- [16] Lyzenga, D. R., “Shallow-water bathymetry using combined lidar and passive multispectral scanner data,” <http://dx.doi.org/10.1080/01431168508948428> **6**(1), 115–125 (1985).
- [17] Dierssen, H. M., Zimmerman, R. C., Leathers, R. A., Downes, T. V. and Davis, C. O., “Ocean color remote sensing of seagrass and bathymetry in the Bahamas Banks by high-resolution airborne imagery,” *Limnol. Oceanogr.* **48**(1part2), 444–455 (2003).
- [18] Hsu, H.-J., Huang, C.-Y., Jasinski, M., Li, Y., Gao, H., Yamanokuchi, T., Wang, C.-G., Chang, T.-M., Ren, H., Kuo, C.-Y. and Tseng, K.-H., “A semi-empirical scheme for bathymetric mapping in shallow water by ICESat-2 and Sentinel-2: A case study in the South China Sea,” *ISPRS J. Photogramm. Remote Sens.* **178**, 1–19 (2021).
- [19] Albert, A. and Mobley, C. D., “An analytical model for subsurface irradiance and remote sensing reflectance in deep and shallow case-2 waters,” *Opt. Express*, Vol. 11, Issue 22, pp. 2873–2890 **11**(22), 2873–2890 (2003).
- [20] Mavraeidopoulos, A. K., Oikonomou, E., Palikaris, A. and Poulos, S., “A Hybrid Bio-Optical Transformation for Satellite Bathymetry Modeling Using Sentinel-2 Imagery,” *Remote Sens.* 2019, Vol. 11, Page 2746 **11**(23), 2746 (2019).
- [21] Hu, L., Liu, Z., Liu, Z., Hu, C. and He, M.-X., “Mapping bottom depth and albedo in coastal waters of the South China Sea islands and reefs using Landsat TM and ETM+ data,” <http://dx.doi.org/10.1080/01431161.2014.916441> **35**(11–12), 4156–4172 (2014).
- [22] Lee, Z., Mobley, C. D., Patch, J. S., Carder, K. L. and Steward, R. G., “Hyperspectral remote sensing for shallow waters. I. A semianalytical model,” *Appl. Opt.* Vol. 37, Issue 27, pp. 6329–6338 **37**(27), 6329–6338 (1998).
- [23] Huang, R., Yu, K., Wang, Y., Wang, J., Mu, L. and Wang, W., “Bathymetry of the Coral Reefs of Weizhou Island Based on Multispectral Satellite Images,” *Remote Sens.* 2017, Vol. 9, Page 750 **9**(7), 750 (2017).
- [24] Marques, F., Eugenio, F., Alfaro, M. and Marcello, J., “Bathymetry Mapping using very High Resolution Satellite Multispectral Imagery in Shallow Coastal Waters of Protected Ecosystems,” *Int. Geosci. Remote Sens. Symp.*, 8234–8237 (2019).
- [25] Lee, Z., Carder, K. L. and Arnone, R. A., “Deriving inherent optical properties from water color: a multiband quasi-analytical algorithm for optically deep waters,” *Appl. Opt.* Vol. 41, Issue 27, pp. 5755–5772 **41**(27), 5755–5772 (2002).
- [26] Gao, J., “Bathymetric mapping by means of remote sensing: methods, accuracy and limitations,” *Prog. Phys. Geogr.* **33**(1), 103–116 (2009).
- [27] Ashphaq, M., Srivastava, P. K. and Mitra, D., “Review of near-shore satellite derived bathymetry: classification and account of five decades of coastal bathymetry research,” *J. Ocean Eng. Sci.* (2021).
- [28] Lyzenga, D. R., “Passive remote sensing techniques for mapping water depth and bottom features,” *Appl. Opt.* Vol. 17, Issue 3, pp. 379–383 **17**(3), 379–383 (1978).
- [29] Stumpf, R. P., Holderied, K. and Sinclair, M., “Determination of water depth with high-resolution satellite imagery over variable bottom types,” *Limnol. Oceanogr.* **48**(1part2), 547–556 (2003).
- [30] Mishra, D. R., Narumalani, S., Rundquist, D. and Lawson, M., “High-resolution ocean color remote sensing of benthic habitats: A case study at the Roatan Island, Honduras,” *IEEE Trans. Geosci. Remote Sens.* **43**(7), 1592–1603 (2005).
- [31] Mohamed, H., Negm, A., Zahran, M. and Saavedra, O. C., “Bathymetry Determination from High Resolution Satellite Imagery Using Ensemble Learning Algorithms in Shallow Lakes: Case Study El-Burullus Lake,” *Int. J. Environ. Sci. Dev.* **7**(4), 295–301 (2016).
- [32] Vojinovic, Z., Abebe, Y. A., Ranasinghe, R., Vacher, A., Martens, P., Mandl, D. J., Frye, S. W., van Ettinger, E. and de Zeeuw, R., “A machine learning approach for estimation of shallow water depths from optical satellite

- images and sonar measurements,” *J. Hydroinformatics* **15**(4), 1408–1424 (2013).
- [33] DoF -Department of Fisheries and Marine Research., “Initial Assessment of the Marine Environment of Cyprus, Part I – Characteristics Nicosia,” Nicosia (2012).
- [34] Aplikioti, M., Markou, M., Stavrou, P., Antoniadis, K., Vasileiou, E., Mixailidis, S., Iosifides, M. and Argirou, M., “Department of Fisheries and Marine Research - Report on Coastal Water Monitoring Program of Cyprus” (2017).
- [35] Department of Lands and Surveys., “DLS Portal,” <<https://portal.dls.moi.gov.cy/en-us/homepage>>.
- [36] International Hydrographic Organization., “IHO Standards for Hydrographic Surveys,” 1–49 (2020).
- [37] SPOT Imagery User Guide., “SPOT Imagery User Guide DEFENCE AND SPACE Intelligence Organisation of the SPOT 6 & SPOT 7 Imagery User Guide” (2013).
- [38] McFeeters, S. K., “The use of the Normalized Difference Water Index (NDWI) in the delineation of open water features,” <https://doi.org/10.1080/01431169608948714> **17**(7), 1425–1432 (1996).
- [39] Kopp, M. and Purgathofer, W., “Efficient 3x3 Median Filter Computations, Technical Report TR-186-2-94-18, Institute of Computer Graphics and Algorithms, Visualization and Animation Group, Vienna University of Technology” (1994).